Temporal interference with frequency-controllable long photons from independent cold atomic sources

Peng Qian,[1] Zhenjie Gu,[1] Rong Wen,[1] Weiping Zhang,[2,3] and J. F. Chen[1,3,*]

[1]*Quantum Institute of Light and Atoms, Department of Physics, East China Normal University, Shanghai 200241, People's Republic of China*

[2]*Department of Physics and Astronomy, Shanghai Jiao Tong University, and Tsung-Dao Lee Institute, Shanghai 200240, People's Republic of China*

[3]*Collaborative Innovation Center of Extreme Optics, Shanxi University, Taiyuan, Shanxi 030006, People's Republic of China*

(Received 26 September 2017; published 4 January 2018)

The interference of single photons from independent sources is an essential tool in quantum information processing. However, the interfering of photons with long temporal states in a time-resolved manner has rarely been studied. This is because without transmitting spectral filters or coupling to a cavity mode single photons generated in traditional nonlinear crystals suffer from a short temporal profile below 1 ns. With spectral correlation maintained in the biphotons generated from spontaneous four-wave mixing process in cold atom clouds, here we demonstrate the temporal interference of two frequency-tunable long photons from two independent cold atomic sources. We observe and analyze the interference of frequency-mismatched photons, where the phenomenon of the quantum beat at megahertz separation is displayed. Our paper provides more details for the quantum beat of two independent narrow-band single photons, which may find potential application in frequency-encoded photonic qubits in quantum information processing.

DOI: 10.1103/PhysRevA.97.013806

I. INTRODUCTION

The interference of single photons from independent sources is a crucial requirement for the implementation of scalable quantum networks [1–4]. When two input single photons meet at a beam splitter (BS), one would expect them to coalesce and leave from the same output port if they are indistinguishable [5]. This requires that the two interfering photons share the same mode in all the degrees of freedom, such as polarization, frequency, spatial-temporal modes, and so on. In practice, matching all these degrees is known to be difficult when two physically different single-photon sources are involved. Usually the photon sources emit correlated photon pairs, where one is used as a trigger and the other is a heralded single photon. Well-developed schemes include spontaneous parametric down-conversion (SPDC) in nonlinear crystals [6,7], spontaneous four-wave mixing (SFWM) in optical fibers [8], and atomic ensembles [9–12]. Hong-Ou-Mandel (HOM) interference is widely observed within the same kind of system [13–19] or hybrid systems [20].

If the interference occurs for single photons with different frequencies (colors), then the interference is termed particularly as a quantum beat, the oscillation period of which is the reciprocal of the frequency difference (FD) between the two photons. This is an important proof of the irreplaceability of full quantum theory compared to semiclassical theory. The phenomenon of the quantum beat has been demonstrated through the photon interference of multiple generation channels in a quantum system [21–24]. A significant consequence of the quantum beat is the generation of frequency-bin entanglement, which utilizes the color degree of freedom of photons and potentially serves as an interface for quantum systems with different excitation frequency. Moreover, the interference curve of the quantum beat is useful in evaluating Bell's inequality factor for frequency-bin entanglement. However, the quantum beat is observed by spatially altering the optical-path difference between photon channels [25,26], because usually the discrepancy of the frequency bin (approximately terahertz) is much larger than the detector bandwidth. To reduce the frequency difference and thus reveal the quantum beat directly in temporal interference, long photons with narrow linewidths are advantageous to avoid spectrum overlap [27,28].

Therefore, the direct observation of temporal interference of single photons requires long photons with coherence time much larger than the detection resolution. In this paper, we take advantage of the narrow-band paired photons generated from SFWM in dense cold atomic clouds [10,29]. In the SFWM process, one of the paired photons is governed by the slow light effect of electromagnetically induced transparency (EIT), and furthermore its central frequency is determined by the EIT window induced by a laser field. By altering the induced EIT window in two different atomic clouds, we produce a quantum beat between two independent single photons from separate clouds. The first feature we emphasize is that the quantum beat is obtained from coincidence measurement directly in the time domain, which is particularly successful with long photons with narrow linewidths. Secondly, the quantum beat signifies the frequency-bin entangled state produced from photons which are independently prepared. The visibility is $81 \pm 2\%$, which is higher than what was reported in other systems [30,31], ascribed to a pure single-photon source and better mode matching among well-separated systems. Finally, based on the narrow-band photon source with controllable

*jfchen@phy.ecnu.edu.cn

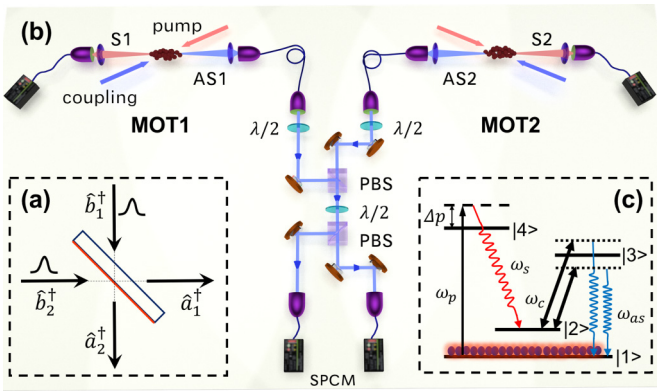

FIG. 1. Experimental setup and energy-level scheme. (a) The scheme of two-photon interference. (b) Experimental setup. Two pairs of photons, Stokes (S) and anti-Stokes (AS), are generated from independent cold atomic systems MOT1 and MOT2, each illuminated by counterpropagating pump and coupling beams. The AS photons of each pair are guided into the interference paths through the polarization-maintaining fibers, while the S photons go directly into single-photon counting modules (SPCM). (c) The SFWM energy-level scheme. The atoms are initially prepared on the ground state $|1\rangle$, and for each system the coupling beam is detuned positive and negative, respectively.

frequency and temporal length, we give detailed discussion about the achievable range of separation in the frequency-bin domain. It is expected that long photons enable a lower bound of the order of megahertz for frequency separation, which may facilitate frequency-encoded photonic qubits in quantum information processing.

II. TEMPORAL INTERFERENCE WITH FREQUENCY-CONTROLLABLE PHOTONS

Generally we consider two single photons in temporal modes $\hat{b}_1(T),\hat{b}_2(T+\tau)$ incident on a beam splitter, where T is the arrival time of photon 1 and τ is the relative time delay of photon 2, as shown in Fig. 1(a). The input two-photon state is $|\Psi_{in}\rangle = \hat{b}_1^\dagger(T)\hat{b}_2^\dagger(T+\tau)|0\rangle$. Now we expand these operators into the frequency domain using

$$\hat{b}_i^\dagger(t) = \int d\omega_i \phi_i^*(\omega_i)\hat{b}_i^\dagger(\omega_i)e^{i\omega_i t}, i = 1,2, \tag{1}$$

where $t = T, T+\tau, \phi_i(\omega_i)$ is the corresponding spectral function of each input single photon and can be normalized as $\int d\omega_i |\phi(\omega_i)|^2 = 1$. The BS gives a transformation of

$$\hat{b}_1^\dagger(\omega_1) = \frac{1}{\sqrt{2}}[i\hat{a}_1^\dagger(\omega_1) + \hat{a}_2^\dagger(\omega_1)], \tag{2}$$

$$\hat{b}_2^\dagger(\omega_2) = \frac{1}{\sqrt{2}}[\hat{a}_1^\dagger(\omega_2) + i\hat{a}_2^\dagger(\omega_2)]. \tag{3}$$

So the output state of the BS is

$$|\Psi_{\text{out}}\rangle = \frac{1}{2}\int d\omega_1 \phi_1^*(\omega_1)e^{i\omega_1 T}\int d\omega_2 \phi_2^*(\omega_2)e^{i\omega_2(T+\tau)} \times [i\hat{a}_1^\dagger(\omega_1)\hat{a}_1^\dagger(\omega_2) - \hat{a}_1^\dagger(\omega_1)\hat{a}_2^\dagger(\omega_2) + \hat{a}_2^\dagger(\omega_1)\hat{a}_1^\dagger(\omega_2) + i\hat{a}_2^\dagger(\omega_1)\hat{a}_2^\dagger(\omega_2)]|0\rangle. \tag{4}$$

Because the function of a photon detector is counting photons' number within its bandwidth, we define a coincidence detection operator as $\hat{D} = \int d\omega_a \int d\omega_b \hat{a}_1^\dagger(\omega_a)\hat{a}_2^\dagger(\omega_b)|0\rangle\langle 0|\hat{a}_2(\omega_b)\hat{a}_1(\omega_a)$, where it is assumed that each detector has a flat frequency response. Here ω_a and ω_b are the detected frequencies in the modes $\hat{a}_1$ and $\hat{a}_2$, respectively. Then we have the coincidence probability

$$P_{12}(\tau) = \langle\Psi_{\text{out}}|\hat{D}|\Psi_{\text{out}}\rangle \tag{5}$$

$$= \frac{1}{4}\int d\omega_a \int d\omega_b |\phi_1(\omega_a)\phi_2(\omega_b)|^2 \times [2 - e^{i(\omega_a-\omega_b)\tau} - e^{-i(\omega_a-\omega_b)\tau}]. \tag{6}$$

In the derivation above, the imaginary terms turn out to be zero, and $\omega_1(\omega_1')$ and $\omega_2(\omega_2')$ have been replaced by the detected frequencies ω_a (mode $\hat{a}_1$ with detector a) or ω_b (mode $\hat{a}_2$ with detector b) accordingly, using the following commutation relations (for $i = 1,2$):

$$[\hat{a}_1(\omega_i),\hat{a}_1^\dagger(\omega_a)] = \delta(\omega_i - \omega_a),$$
$$[\hat{a}_2(\omega_i),\hat{a}_2^\dagger(\omega_b)] = \delta(\omega_i - \omega_b). \tag{7}$$

Because we only measure the case where both detectors click, the values of ω_a and ω_b can be only chosen between ω_1 and ω_2. To induce the beat signal pattern, we introduce a frequency shift Δ to each of the two independent photons as $\omega_1 = \omega_0 + \Delta_1 + \omega, \omega_2 = \omega_0 + \Delta_2 + \omega$, where ω denotes deviation from the central frequency $\omega_0 + \Delta_{1(2)}$. When the spectral functions are rewritten as $\phi_1(\omega)$ and $\phi_2(\omega)$, the coincidence probability can be simplified as

$$P_{12}(\tau) = \frac{1}{2}\int d\omega|\phi_1(\omega)|^2 \int d\omega|\phi_2(\omega)|^2 - \frac{1}{4}2\pi\frac{1}{2\pi} \times \int d\omega|\phi_1(\omega)|^2 e^{-i\omega\tau}\int d\omega|\phi_2(\omega)|^2 e^{i\omega\tau}e^{i(\Delta_2-\Delta_1)\tau} - \frac{1}{4}2\pi\frac{1}{2\pi}\int d\omega|\phi_1(\omega)|^2 e^{i\omega\tau} \times \int d\omega|\phi_2(\omega)|^2 e^{-i\omega\tau}e^{-i(\Delta_2-\Delta_1)\tau} \tag{8}$$

$$= \frac{1}{2} - \frac{1}{2}2\pi\mathcal{F}[|\phi_1(\omega)|^2]\mathcal{F}[|\phi_2(\omega)|^2]\cos(\Delta\omega\tau). \tag{9}$$

Here $e^{-i\omega_0\tau}$ and $e^{i\omega_0\tau}$ cancel each other out, and $\Delta\omega = \Delta_2 - \Delta_1$ is the angular frequency difference between the photons. $\mathcal{F}[|\phi_i(\omega)|^2] = 1/\sqrt{2\pi}\int d\omega|\phi_i(\omega)|^2 e^{-i\omega\tau}$ indicates the Fourier transformation of the spectral function. Note that the spectral functions ϕ_i here are even symmetric, i.e., $\phi_i(\omega) = \phi_i(-\omega), i = 1,2$, and the Fourier and inverse Fourier transformations are equivalent. Also we are able to manipulate the systems to guarantee spectral functions of the independent long photons to be nearly identical, i.e., $\phi_1(\omega) \approx \phi_2(\omega)$. This is achieved by manipulating the coupling beam power and the atomic optical depth in each SFWM to match the measured cross-correlation function, proportional to $\mathcal{F}[|\phi_i(\omega)|^2]$, of the two independent sources of paired photons. The similarity between them in our system can be maintained as $97\% \pm 2\%$. It will degrade the interference visibility by the scaling factor which is equal to the nonunity similarity, and thus reduce the purity of the generated entangled state. Equation (9) shows

that, when $\Delta\omega = 0$, the Hong-Ou-Mandel dip at $\tau = 0$ indicating the typical two-photon interference is obtained. For the interference between two frequency-mismatched independent single-photon wave packets, the quantum beat is indicated in the term $\cos(\Delta\omega\tau)$. When $\Delta\omega$ grows larger, a stronger oscillation will be added to the dip envelope.

As shown in Fig. 1(b), two pairs of time-frequency entangled photons are generated in two independent ^{85}Rb cold atomic clouds, which are prepared in two sets of two-dimensional magneto-optical traps [32,33] (MOT1 and MOT2), respectively. Each of the clouds is illuminated by two counterpropagating laser fields denoted as pump (780 nm) and coupling field (795 nm) at an angle of 3° with respect to the longitudinal axis. Different from the pulsed pumping scheme, our pump and coupling fields are running continuously during the photon generation window of 0.5 ms, which is following a MOT preparation time of 4.5 ms. These two fields stimulate a SFWM process, and according to the phase matching condition a pair of photons, the Stokes (S, 780 nm) and anti-Stokes (AS, 795 nm) photons, are generated. They travel along the longitudinal axis in opposite directions and are collected in single-mode fibers (SMFs). The atomic energy-level scheme is represented by a double-Λ four-level system as shown in Fig. 1(c). The atoms are originally prepared at the ground state $|1\rangle = 5S_{1/2}, F = 2$, then pumped by a weak pump beam into a virtual state which is blue detuned from $|4\rangle = 5P_{3/2}, F = 3$ by $\Delta_p = 2\pi \times 146$ MHz. The Rabi frequency of the pump field is $\Omega_p = 2\pi \times 1.4$ MHz. Instead of being on resonance with the transition $|2\rangle = 5S_{1/2}, F = 3 \rightarrow |3\rangle = 5P_{1/2}, F = 3$, here each coupling field is detuned by an amount of frequency. The Rabi frequency of the coupling field is $\Omega_c = 2\pi \times 17$ MHz. Correspondingly, the frequency of AS photons from MOT1 is shifted positively and that of MOT2 is shifted negatively, from the transition $|3\rangle \rightarrow |1\rangle$. Here, due to the strong EIT effect, the AS photons go through a narrow EIT window with an adjustable time delay relative to the S photons. Therefore, by controlling the slow light effect, long coherence time of even microsecond scale can be generated in such scheme, without any extra filtering or cavities [29,34]. Since such long coherence time is easily resolved by most commercial photon detectors, the heralded AS photons are projected into a nearly pure single-photon state [15,35], which guarantees the interference of photons from independent sources. In this double Λ atomic system, the residue magnetic field causes the nondegeneracy for the Zeeman levels, which causes a nonzero two-photon detuning and thus reduces the paired photon generation rate. Also, the coherence time of the photon pairs will be affected by a serious Zeeman splitting. Therefore we will optimize the position of the atomic cloud and thus minimize the effect of residue magnetic field.

In the setup described above, the production rate of the paired photons generated from each MOT is 30 000/s, which is significantly greater than the dark count rate 250/s of the single-photon counting modules (SPCMs). The trigger photons S1 and S2 go directly into SPCMs, while the photons AS1 and AS2 are imported into the interference optical paths. As shown in Fig. 1(b), the two beams of AS photons, the polarizations of which are, respectively, rotated as horizontal and vertical, are first combined at a polarization beam splitter (PBS). Then both of their polarizations are rotated clockwise (or anticlockwise) by 45° through a half-wave plate before a second PBS where the two beams are mixed. Therefore the second PBS acts as a 50 : 50 beam splitter, the splitting ratio of which can be fine tuned by the half-wave plate. After interference, the AS photons are also collected by another two SPCMs.

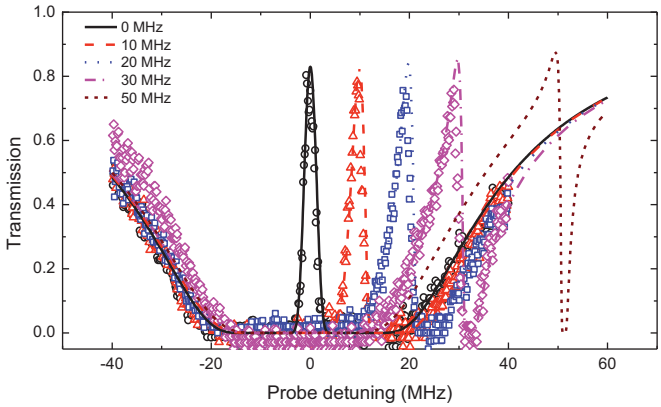

FIG. 2. Measurements for the EIT spectrum at different coupling frequency detunings with OD = 120. The circles, triangles, squares, and diamonds mark the experimental data at different detunings, with lines denoting corresponding theoretical curves. The brown short dashed line is out of our capability of measurement.

With the phase-matching condition of the SFWM process, the frequency of single photons can be altered by detuning the coupling beams [36]. Compared to the solid-state system, e.g., SPDC with temperature-varying approach [26] and the quantum dots and Nitrogen vacancy (NV) centers [18,19], the manipulation in the atomic cloud is much less demanding and more accurate. But the tunable frequency range is constrained by the EIT spectrum, otherwise both real and imaginary parts of the linear susceptibility will be changed severely, and the EIT spectrum will be distorted. To show this, we measured the transmission spectrum of a weak (40 nW) probe beam, which travels through the cold atomic cloud and is scanned from -40 to $+40$ MHz with respect to the transition $|1\rangle \rightarrow |3\rangle$. The coupling beam is on resonance or blue detuned from 10 to 50 MHz. As shown in Fig. 2, at 20-MHz detuning of the coupling beam, where it is the edge of the flat bottom of the probe transmission spectrum, the width of the transparency window (blue peak) is still not significantly different from that in the resonant case (black peak). In contrast, the transparency windows are distorted seriously when the coupling detuning is larger than 20 MHz. Although the peak of the transparency window stays high for even far detuning of 50 MHz, the slow light effect will be diminished and the temporal biphoton waveform will be shortened and deformed significantly. In this case, the temporal-mode indistinguishability and purity of the two independent single photons are not guaranteed any more. Noting that those measurements in Fig. 2 are operated at an optical depth (OD) of only 120, the problems discussed above can be improved by increasing OD. For example, an ultrahigh OD of 264 is able to be achieved with "dark-line" technique [37], which can extend $\Delta_{1(2)}$ to be about ± 30 MHz. Here it is defined that OD $= N\sigma_0 L$, where N denotes the atomic density, σ_0 denotes the resonant absorption cross section [38], and L is the effective interaction length. Therefore, the acceptable

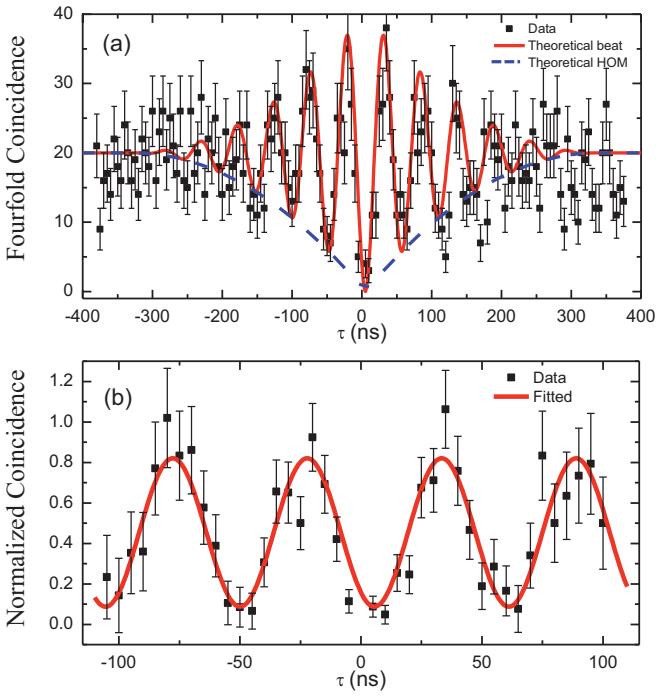

FIG. 3. Observation of the quantum beat between two independent AS photons the frequencies of which are detuned by $+10$ and -10 MHz, respectively. (a) Accumulated fourfold coincidence with 5 ns as the time step. The experimental data are denoted by black filled squares with error bars. The red solid lines denote the theoretical result from Eq. (9), which is enveloped by the HOM dip curve denoted by the blue dashed line. (b) Normalized beating signal with data in (a) from $\tau = -100$ to 100 ns. The solid curve shows the best fitting.

free detuning range of the coupling frequency in our scheme is limited by the EIT spectrum for the AS photons, and is thus mainly determined by OD of the atom cloud.

The interference result in Fig. 3(a) shows a typical quantum beat signal of frequency-mismatched photons with the arrival time difference τ as the horizontal axis. Here the frequency detunings of the coupling beams are $\Delta_1 = +2\pi \times 10$ MHz and $\Delta_2 = -2\pi \times 10$ MHz, respectively, and the temporal length of both photons is about 150 ns. The coincidence counts take a minimum value at $\tau = 0$ when two single photons coincide. The theoretical curve is obtained from Eq. (9), in which the spectral function $\phi(\omega)$ is considered as a sinc function according to the phase-matching condition of the SFWM process in cold atoms [10]. $\Delta\omega$ in Eq. (9) is fitted as 19 MHz from the experimental oscillation curve. This discrepancy comes from the ac-Stark shift of the atomic energy state induced by the strong-coupling field. To show the relation between the beating curve and the corresponding HOM dip, the theoretical curve according to Eq. (9) with $\Delta\omega = 0$ is also indicated in the plot. Both the ideal HOM interference and the quantum beat give coincidence counts as zero at $\tau = 0$. We normalize the beating signal to the ideal HOM-dip envelope between -100 and 100 ns and fit it with a cosine function. As shown in Fig. 3(b), the visibility from numerical fitting is $V = 81 \pm 2\%$ without subtracting the multiphoton events and accidental counts. This visibility exceeds the classical limit 50%, and is ascribed to the pure nonclassical single-photon sources we produce from MOTs. In experiment, this purity is guaranteed by the low second-order autocorrelation functions of $g_1^{(2)} = 0.193 \pm 0.004$ and $g_2^{(2)} = 0.196 \pm 0.004$ for MOT1 and MOT2, which are mainly caused by multiphoton events and contribute to the nonzero accidental counts which lead to a reduction of interference visibility [15]. Therefore, with long enough coherence time and resolvable beating period, the interference between independent single photons is observed directly in the time domain.

III. LIMITS OF FREQUENCY SEPARATION OF DISCRETE FREQUENCY-BIN ENTANGLED STATES

Since either of the anti-Stokes photons from MOT1 and MOT2 has equal probability to exit from the transmission and reflection port of the BS, the two photons generated from the output ports of BS are entangled in a basis constituted from two well-separated frequency-bin states. By postselecting coincidence events between the output ports of BS, we can have a discrete-frequency entangled state

$$|\Psi_{\text{ent}}\rangle = \frac{1}{\sqrt{2}}[|1(\omega_2)1(\omega_1)\rangle - e^{\pm i\Delta\omega\tau}|1(\omega_1)1(\omega_2)\rangle], \quad (10)$$

where $|1(\omega_1)\rangle = 1/2^{1/4}\int d\omega\phi_1^*(\omega)\hat{a}_i^\dagger(\omega)e^{i\omega T}|0\rangle, |1(\omega_2)\rangle = \int d\omega\phi_2^*(\omega)\hat{a}_i^\dagger(\omega)e^{i\omega(T+\tau)}|0\rangle$, ω is a frequency deviation for integration, and $i = 1,2$ indicates whether the photon is in output mode a_1 or a_2. $\Delta\omega = \omega_2 - \omega_1$ is the frequency difference between the two photons. For detailed derivation, please refer to the Appendix. This is the antisymmetric Bell state with a phase difference $e^{\pm i\Delta\omega\tau}$. Here the temporal interference we observed in the quantum beat experiment, described by Eq. (9), is equivalent to the two-photon coincidence fringes obtained from polarization entangled paired photons [39,40]. The visibility of $81 \pm 2\%$ for the temporal beating signal in Fig. 3 indicates a violation of the Bell inequality, and predicts the Clauser-Horne-Shimony-Holt-type Bell parameter as $|S| = 2\sqrt{2}V = 2.29$.

Here the minus sign in Eq. (10) between the two states naturally results from the transformation of the BS, and contributes to a destructive interference between the two output paths at $\tau = 0$. This is different from the color-entangled state in Ref. [26], where when the entangled two photons interfere at the second BS the coincidence reaches a maximal value at $\tau = 0$ and signifies an unambiguous antisymmetric feature. Actually, if only the $|\Psi^-\rangle$ Bell state is desired, our interference setup is a discrete-frequency entanglement generator with two independent sources, on the condition that the time delay τ is much smaller than the temporal length of the individual photons. On the other hand, our long temporal length of photons and continuous excitation fields save us the trouble of manually varying the relative arrival times of the interfering photons in observing the interference pattern. In Fig. 3(a), the coincidence starts to oscillate when τ increases, and reaches every maximal value at about $|\tau| = \pi(2m+1)/\Delta\omega, m = 0,1,\ldots$, where the entangled state reaches its best generation probability around that delay. From this point of view, by using a temporal filter only to select photons with $\tau = 0$, or actively compensating the phase delay with time-resolved measurements, the two frequency-mismatched photons can keep their coherence all

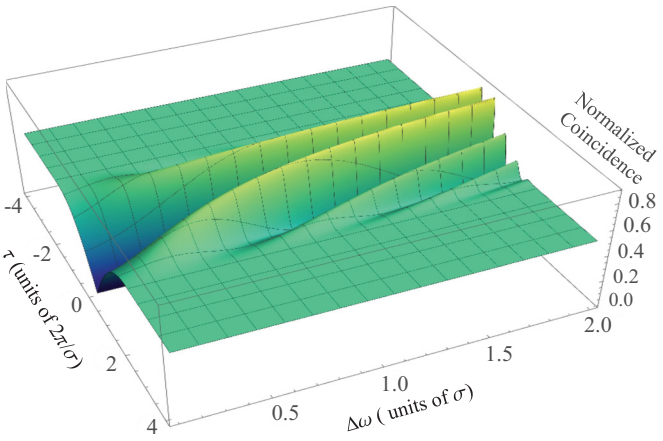

FIG. 4. Three-dimensional plotting of normalized coincidence as a function of both time delay and frequency difference (FD), $\Delta\omega$, between two photons with Eq. (9). The unit of the FD axis is the photon bandwidth (σ). When $\Delta\omega = 0$, the typical HOM dip appears.

the time and avoid exiting from different output ports, as has been proposed and implemented by other groups [41,42]. It is interesting to notice that the frequency-bin entanglement without postselection may be also achieved in our systems with the same methods, by keeping only those input photons with $\tau = \pi/\Delta\omega$ before the BS. In this preselection way, the two photons will almost deterministically go different ways.

In the experiment, the angular FD $\Delta\omega$ between the two beating single photons is set to be $2\pi \times 20$ MHz. But what is the range of it? Generally, the largest FD is limited by the detection bandwidth of the single-photon detector. The beating signal will be averaged out by slow detectors. But specifically in our system, the upper bound is mainly confined by the maximum coupling frequency detuning, as discussed in Sec. II. On the other hand, how small can the FD be? To show this, we plot in Fig. 4 the normalized coincidence as a function of both time delay and the angular FD according to Eq. (9), using the photon spectral function $\phi(\omega) = 1/\sqrt{\sigma\pi}\,\mathrm{sinc}(\omega/\sigma)$, where σ is the photon bandwidth. It is clearly seen that, when $\Delta\omega$ decreases from a large value, pairs of "mountain ridges" (oscillations) decline and the "valley" opens larger. If $\Delta\omega$ is smaller than about half of σ, obvious oscillations are swallowed by the uncertainty within the photon bandwidth and can be hardly seen any more. This indicates that the FD cannot be resolved by the single photons with current bandwidth, unless photons of even narrower bandwidth are employed. Therefore, the quantum beat can be used to test the bandwidth of two input photons onto a BS by narrowing down the FD until oscillations start to vanish, which is when the FD is comparable with the photon bandwidth. This smallest distinguishable FD can be called the "beating resolution."

According to the fitting, the bandwidth of the interfering photons used in Fig. 3 is $\sigma \approx 2\pi \times 6$ MHz, much smaller than $\Delta\omega = 2\pi \times 20$ MHz. Hence these two well-separated frequency modes are orthogonal, which is useful to construct a frequency-bin qubit. Different from the SPDC scheme, the frequency separation of photons from our systems is of the order of megahertz, which is easily detected through current technology of time-resolving detection. This is also still a challenge for quantum dots and NV centers, the spectral separations of which are usually of gigahertz or terahertz level between different sources. If we decrease the photon bandwidth down to $2\pi \times 0.38$ MHz by increasing the OD and employing appropriate coupling light intensity [29], the frequency separation can be as small as hundreds of kilohertz with the two photons still well separated in the spectrum. Therefore, taking great advantage of frequency controllable long photons in our systems, the lower bound of the FD can be extended, which is beneficial for dense coding of frequency bins in quantum information science [43].

IV. CONCLUSION

In summary, we have experimentally demonstrated temporal interference showing the quantum beat with frequency-mismatched photons heralded from the SFWM process in two independent cold atomic sources. We obtained a visibility of $81 \pm 2\%$, which well exceeds the classical limit. The frequency difference is of megahertz scale which is easily time resolved by most commercial single-photon detectors, and the frequency detuning range of the single photons generated in our scheme is limited by the OD. Temporal interference of longer photons can distinguish small frequency difference, e.g., of the order of megahertz scale. Conversely, by narrowing down the frequency difference, the bandwidth of the photons can be roughly tested. The setup reported in this paper is a scheme to entangle two independent single photons in a basis of two discrete frequencies, which is useful in quantum information science. Furthermore, time-resolved detection with long photons has been proved to be powerful in producing pure heralded single photons [15], entanglement swapping [44], biphoton entanglement [42], and Bell inequality testing [40]. It is promising that photons with long coherence time are useful to characterize the frequency-bin entangled states directly in the time domain.

ACKNOWLEDGMENTS

The authors thank Prof. Z. Y. Ou for helpful discussion. This paper is supported by the National Key Research and Development Program of China under Grant No. 2016YFA0302001; the National Natural Science Foundation of China under Grants No. 11674100, No. 11654005, and No. 11234003; the Natural Science Foundation of Shanghai under Grant No. 16ZR1448200; and Shanghai Rising-Star Program No. 17QA1401300.

APPENDIX

As shown in Fig. 5, generally we consider two single photons in temporal modes $\hat{b}_1(T), \hat{b}_2(T+\tau)$ incident on a beam splitter, where T is the arriving time of photon 1 and τ is the relative time delay of photon 2. Then the input two-photon state is $|\Psi_{\mathrm{in}}\rangle = \hat{b}_1^\dagger(T)\hat{b}_2^\dagger(T+\tau)|0\rangle$. Now we expand these operators into the frequency domain using

$$\hat{b}_i^\dagger(t) = \int d\omega_i \phi_i^*(\omega_i)\hat{b}_i^\dagger(\omega_i)e^{i\omega_i t}, \tag{A1}$$

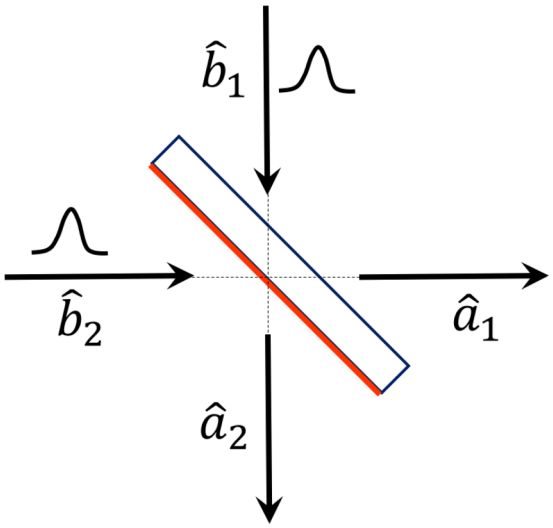

FIG. 5. Two single photons incident on a beam splitter.

where $i = 1,2$, $\phi_i(\omega_i)$ is the corresponding spectral function of each input single photon and can be normalized as $\int d\omega_i |\phi(\omega_i)|^2 = 1$. Then $|\Psi_{\text{in}}\rangle$ can be represented as

$$|\Psi_{\text{in}}\rangle = \int d\omega_1 \phi_1^*(\omega_1)\hat{b}_1^\dagger(\omega_1)e^{i\omega_1 T} \cdot \int d\omega_2 \phi_2^*(\omega_2)\hat{b}_2^\dagger(\omega_2)e^{i\omega_2(T+\tau)}|0\rangle. \tag{A2}$$

The BS gives a transformation of

$$\hat{b}_1^\dagger(\omega_1) = \frac{1}{\sqrt{2}}[i\hat{a}_1^\dagger(\omega_1) + \hat{a}_2^\dagger(\omega_1)], \tag{A3}$$

$$\hat{b}_2^\dagger(\omega_2) = \frac{1}{\sqrt{2}}[\hat{a}_1^\dagger(\omega_2) + i\hat{a}_2^\dagger(\omega_2)]. \tag{A4}$$

So the output state of the BS is

$$|\Psi_{\text{out}}\rangle = \frac{1}{2}\int d\omega_1 \phi_1^*(\omega_1)[i\hat{a}_1^\dagger(\omega_1) + \hat{a}_2^\dagger(\omega_1)]e^{i\omega_1 T}\int d\omega_2 \phi_2^*(\omega_2)[\hat{a}_1^\dagger(\omega_2) + i\hat{a}_2^\dagger(\omega_2)]e^{i\omega_2(T+\tau)}|0\rangle \tag{A5}$$

$$= \frac{1}{2}\int d\omega_1 \phi_1^*(\omega_1)e^{i\omega_1 T}\int d\omega_2 \phi_2^*(\omega_2)e^{i\omega_2(T+\tau)} \times [i\hat{a}_1^\dagger(\omega_1)\hat{a}_1^\dagger(\omega_2) - \hat{a}_1^\dagger(\omega_1)\hat{a}_2^\dagger(\omega_2) + \hat{a}_2^\dagger(\omega_1)\hat{a}_1^\dagger(\omega_2) + i\hat{a}_2^\dagger(\omega_1)\hat{a}_2^\dagger(\omega_2)]|0\rangle. \tag{A6}$$

Because the function of a photon detector is counting photons' number within its bandwidth, we define a coincidence detection operator as $\hat{D} = \int d\omega_a \int d\omega_b \hat{a}_1^\dagger(\omega_a)\hat{a}_2^\dagger(\omega_b)|0\rangle\langle 0|\hat{a}_2(\omega_b)\hat{a}_1(\omega_a)$, where it is assumed that each detector has a flat frequency response. Here ω_a and ω_b are the detected frequencies in the modes $\hat{a}_1$ and $\hat{a}_2$, respectively. Then we have the coincidence probability

$$P_{12}(\tau) = \langle\Psi_{\text{out}}|\hat{D}|\Psi_{\text{out}}\rangle \tag{A7}$$

$$= \frac{1}{2}\langle 0|\int d\omega_1' \phi_1(\omega_1')e^{-i\omega_1' T}\int d\omega_2' \phi_2(\omega_2')e^{-i\omega_2'(T+\tau)}[-i\hat{a}_1(\omega_1')\hat{a}_1(\omega_2') - \hat{a}_1(\omega_1')\hat{a}_2(\omega_2') + \hat{a}_2(\omega_1')\hat{a}_1(\omega_2') - i\hat{a}_2(\omega_1')\hat{a}_2(\omega_2')]\int d\omega_a \int d\omega_b \hat{a}_1^\dagger(\omega_a)\hat{a}_2^\dagger(\omega_b)|0\rangle\langle 0|\hat{a}_2(\omega_b)\hat{a}_1(\omega_a)\frac{1}{2}\int d\omega_1 \phi_1^*(\omega_1)e^{i\omega_1 T} \times \int d\omega_2 \phi_2^*(\omega_2)e^{i\omega_2(T+\tau)}[i\hat{a}_1^\dagger(\omega_1)\hat{a}_1^\dagger(\omega_2) - \hat{a}_1^\dagger(\omega_1)\hat{a}_2^\dagger(\omega_2) + \hat{a}_2^\dagger(\omega_1)\hat{a}_1^\dagger(\omega_2) + i\hat{a}_2^\dagger(\omega_1)\hat{a}_2^\dagger(\omega_2)]|0\rangle \tag{A8}$$

$$= \frac{1}{4}\int d\omega_a \int d\omega_b \langle 0|[-\int d\omega_1' \phi_1(\omega_1')\hat{a}_1(\omega_1')\hat{a}_1^\dagger(\omega_a)e^{-i\omega_1' T}\int d\omega_2' \phi_2(\omega_2')\hat{a}_2(\omega_2')\hat{a}_2^\dagger(\omega_b)e^{-i\omega_2'(T+\tau)} + \int d\omega_1' \phi_1(\omega_1')\hat{a}_2(\omega_1')\hat{a}_2^\dagger(\omega_b)e^{-i\omega_1' T}\int d\omega_2' \phi_2(\omega_2')\hat{a}_1(\omega_2')\hat{a}_1^\dagger(\omega_a)e^{-i\omega_2'(T+\tau)}]|0\rangle \times \langle 0|[-\int d\omega_1 \phi_1^*(\omega_1)\hat{a}_1(\omega_a)\hat{a}_1^\dagger(\omega_1)e^{i\omega_1 T}\int d\omega_2 \phi_2^*(\omega_2)\hat{a}_2(\omega_b)\hat{a}_2^\dagger(\omega_2)e^{i\omega_2(T+\tau)} + \int d\omega_1 \phi_1^*(\omega_1)\hat{a}_2(\omega_b)\hat{a}_2^\dagger(\omega_1)e^{i\omega_1 T}\int d\omega_2 \phi_2^*(\omega_2)\hat{a}_1(\omega_a)\hat{a}_1^\dagger(\omega_2)e^{i\omega_2(T+\tau)}|0\rangle \tag{A9}$$

$$= \frac{1}{4}\int d\omega_a \int d\omega_b[-\phi_1(\omega_a)e^{-i\omega_a T}\phi_2(\omega_b)e^{-i\omega_b(T+\tau)} + \phi_1(\omega_b)e^{-i\omega_b T}\cdot\phi_2(\omega_a)e^{-i\omega_a(T+\tau)}] \times [-\phi_1^*(\omega_a)e^{i\omega_a T}\cdot\phi_2^*(\omega_b)e^{i\omega_b(T+\tau)} + \phi_1^*(\omega_b)e^{i\omega_b T}\cdot\phi_2^*(\omega_a)e^{i\omega_a(T+\tau)}] \tag{A10}$$

$$= \frac{1}{4}\int d\omega_a \int d\omega_b |\phi_1(\omega_a)\phi_2(\omega_b)|^2[e^{-i\omega_b T}e^{-i\omega_a(T+\tau)} - e^{-i\omega_a T}e^{-i\omega_b(T+\tau)}][e^{i\omega_b T}e^{i\omega_a(T+\tau)} - e^{i\omega_a T}e^{i\omega_b(T+\tau)}] \tag{A11}$$

$$= \frac{1}{4}\int d\omega_a \int d\omega_b |\phi_1(\omega_a)\phi_2(\omega_b)|^2 [e^{-i\omega_a\tau} - e^{-i\omega_b\tau}][e^{i\omega_a\tau} - e^{i\omega_b\tau}] \tag{A12}$$

$$= \frac{1}{4}\int d\omega_a \int d\omega_b |\phi_1(\omega_a)\phi_2(\omega_b)|^2 [2 - e^{i(\omega_a-\omega_b)\tau} - e^{-i(\omega_a-\omega_b)\tau}]. \tag{A13}$$

In the derivation above, the imaginary terms turn out to be zero, and $\omega_1(\omega_1')$ and $\omega_2(\omega_2')$ have been replaced by the detected frequencies ω_a (mode $\hat{a}_1$ with detector a) or ω_b (mode $\hat{a}_2$ with detector b) accordingly, using the following commutation relations (for $i = 1,2$):

$$[\hat{a}_1(\omega_i),\hat{a}_1^\dagger(\omega_a)] = \delta(\omega_i - \omega_a),[\hat{a}_2(\omega_i), \quad \hat{a}_2^\dagger(\omega_b)] = \delta(\omega_i - \omega_b). \tag{A14}$$

Because we only select the case where both detectors click, the values of ω_a and ω_b can be only chosen between ω_1 and ω_2. Therefore the final coincidence probability is given by

$$P_{12}(\tau) = \frac{1}{4}\int d\omega_1 \int d\omega_2 |\phi_1(\omega_1)\phi_2(\omega_2)|^2 (2 - e^{i(\omega_2-\omega_1)\tau} - e^{-i(\omega_2-\omega_1)\tau}) \tag{A15}$$

$$= \frac{1}{2}\int d\omega_1 |\phi_1(\omega_1)|^2 \int d\omega_2 |\phi_2(\omega_2)|^2 - \frac{1}{4}2\pi\frac{1}{2\pi}\int d\omega_1 |\phi_1(\omega_1)|^2 e^{-i\omega_1\tau}\int d\omega_2 |\phi_2(\omega_2)|^2 e^{i\omega_2\tau}$$
$$- \frac{1}{4}2\pi\frac{1}{2\pi}\int d\omega_1 |\phi_1(\omega_1)|^2 e^{i\omega_1\tau}\int d\omega_2 |\phi_2(\omega_2)|^2 e^{-i\omega_2\tau}. \tag{A16}$$

In experiments and applications involving photon interference, indistinguishable photons are usually required, which means here $\omega_1 = \omega_2 = \omega_0$. Now we introduce some frequency shift to each of the two independent photons as $\omega_1 = \omega_0 + \omega + \Delta_1, \omega_2 = \omega_0 + \omega + \Delta_2$, and rewrite the spectral functions as $\phi_1(\omega),\phi_2(\omega)$, where ω denotes the deviation from the central frequency $\omega_0 + \Delta_{1(2)}$; then we have

$$P_{12}(\tau) = \frac{1}{2}\int d\omega |\phi_1(\omega)|^2 \int d\omega |\phi_2(\omega)|^2 - \frac{1}{4}2\pi\frac{1}{2\pi}\int d\omega |\phi_1(\omega)|^2 e^{-i\omega\tau}\int d\omega |\phi_2(\omega)|^2 e^{i\omega\tau} e^{i(\Delta_2-\Delta_1)\tau}$$
$$- \frac{1}{4}2\pi\frac{1}{2\pi}\int d\omega |\phi_1(\omega)|^2 e^{i\omega\tau}\int d\omega |\phi_2(\omega)|^2 e^{-i\omega\tau} e^{-i(\Delta_2-\Delta_1)\tau}, \tag{A17}$$

where $e^{-i\omega_0\tau}$ and $e^{i\omega_0\tau}$ cancel each other out. Usually it is reasonable to assume that the spectral functions here are even symmetric, i.e., $\phi_i(\omega) = \phi_i(-\omega), i = 1,2$. For such functions, the Fourier and inverse Fourier transforms are the same obviously. So the coincidence probability can be simplified as

$$P_{12}(\tau) = \frac{1}{2}\left|\int d\omega |\phi(\omega)|^2\right|^2 - \frac{1}{4}2\pi\frac{1}{2\pi}\int d\omega |\phi_1(\omega)|^2 e^{-i\omega\tau}\int d\omega |\phi_2(\omega)|^2 e^{-i\omega\tau}[e^{i(\Delta_2-\Delta_1)\tau} + e^{-i(\Delta_2-\Delta_1)\tau}]$$
$$= \frac{1}{2}\left|\int d\omega |\phi(\omega)|^2\right|^2 - \frac{1}{2}2\pi F[|\phi_1(\omega)|^2]F[|\phi_2(\omega)|^2]\cos(\Delta\omega\tau). \tag{A18}$$

Here $\Delta\omega = \Delta_2 - \Delta_1$ indicates the frequency difference between two photons. Now we have the function that describes the interference effect of two frequency mismatched independent single-photon wave packets. When $\Delta\omega = 0$, we will obtain the Hong-Ou-Mandel dip. When $\Delta\omega$ is larger, a stronger oscillation will be added to the dip envelope.

Because our interfering photons are well separated in central frequencies, by postselecting the coincidence events between the output ports of the BS, we can have a discrete-frequency entangled state

$$|\Psi_{\text{ent}}\rangle = \int d\omega_a \int d\omega_b \hat{a}_1^\dagger(\omega_a)\hat{a}_2^\dagger(\omega_b)|0\rangle\langle 0|\hat{a}_2(\omega_b)\hat{a}_1(\omega_a)|\Psi_{\text{out}}\rangle$$
$$= \frac{1}{2}\int d\omega_a \int d\omega_b \hat{a}_1^\dagger(\omega_a)\hat{a}_2^\dagger(\omega_b)|0\rangle\langle 0|\hat{a}_2(\omega_b)\hat{a}_1(\omega_a)\int d\omega_1 \phi_1^*(\omega_1)e^{i\omega_1 T}\int d\omega_2 \phi_2^*(\omega_2)e^{i\omega_2(T+\tau)}$$
$$\times [i\hat{a}_1^\dagger(\omega_1)\hat{a}_1^\dagger(\omega_2) - \hat{a}_1^\dagger(\omega_1)\hat{a}_2^\dagger(\omega_2) + \hat{a}_2^\dagger(\omega_1)\hat{a}_1^\dagger(\omega_2) + i\hat{a}_2^\dagger(\omega_1)\hat{a}_2^\dagger(\omega_2)]|0\rangle$$
$$= \frac{1}{2}\int d\omega_a \int d\omega_b \hat{a}_1^\dagger(\omega_a)\hat{a}_2^\dagger(\omega_b)[\phi_1^*(\omega_b)\phi_2^*(\omega_a)e^{i\omega_b T}e^{i\omega_a(T+\tau)} - \phi_1^*(\omega_a)\phi_2^*(\omega_b)e^{i\omega_a T}e^{i\omega_b(T+\tau)}]|0\rangle$$
$$= \frac{1}{2}\Bigg[\int d\omega_a \phi_2^*(\omega_a)\hat{a}_1^\dagger(\omega_a)e^{i\omega_a(T+\tau)}\int d\omega_b \phi_1^*(\omega_b)\hat{a}_2^\dagger(\omega_b)e^{i\omega_b T}$$
$$- \int d\omega_a \phi_1^*(\omega_a)\hat{a}_1^\dagger(\omega_a)e^{i\omega_a T}\int d\omega_b \phi_2^*(\omega_b)\hat{a}_2^\dagger(\omega_b)e^{i\omega_b(T+\tau)}\Bigg]|0\rangle$$

$$= \frac{1}{2}\Big[\int d\omega\phi_2^*(\omega)\hat{a}_1^\dagger(\omega)e^{i(\overline{\omega}_a+\omega)(T+\tau)}\int d\omega\phi_1^*(\omega)\hat{a}_2^\dagger(\omega)e^{i(\overline{\omega}_b+\omega)T}$$
$$- \int d\omega\phi_1^*(\omega)\hat{a}_1^\dagger(\omega)e^{i(\overline{\omega}_a+\omega)T}\int d\omega\phi_2^*(\omega)\hat{a}_2^\dagger(\omega)e^{i(\overline{\omega}_b+\omega)(T+\tau)}\Big]|0\rangle$$
$$= \frac{1}{2}e^{i\overline{\omega}_a(T+\tau)}e^{i\overline{\omega}_bT}\Big[\int d\omega\phi_2^*(\omega)\hat{a}_1^\dagger(\omega)e^{i\omega(T+\tau)}\int d\omega\phi_1^*(\omega)\hat{a}_2^\dagger(\omega)e^{i\omega T}$$
$$- e^{i(\overline{\omega}_b-\overline{\omega}_a)\tau}\int d\omega\phi_1^*(\omega)\hat{a}_1^\dagger(\omega)e^{i\omega T}\int d\omega\phi_2^*(\omega)\hat{a}_2^\dagger(\omega)e^{i\omega(T+\tau)}\Big]|0\rangle. \quad \text{(A19)}$$

Here we used $\omega_{a(b)} = \overline{\omega}_{a(b)} + \omega$, where $\overline{\omega}_{a(b)}$ is the central frequency and ω is the deviation for integration. Notice that ϕ_i^* is the spectral function of the photon with frequency $\omega_i, i = 1,2$; therefore, for example, $\int d\omega\phi_2^*(\omega)\hat{a}_1^\dagger(\omega)e^{i\omega T}|0\rangle$ means the detected photon at mode $\hat{a}_1$ is the one with frequency ω_2. So the entangled state can be rewritten as

$$|\Psi_{\text{ent}}\rangle = e^{i\xi}\frac{1}{\sqrt{2}}[|1(\omega_2)1(\omega_1)\rangle - e^{\pm i\Delta\omega\tau}|1(\omega_1)1(\omega_2)\rangle], \quad \text{(A20)}$$

where $\xi = \overline{\omega}_a(T+\tau) + \overline{\omega}_bT$, and $|1(\omega_1)\rangle = 1/2^{1/4}\int d\omega\phi_1^*(\omega)\hat{a}_i^\dagger(\omega)e^{i\omega T}|0\rangle, |1(\omega_2)\rangle = \int d\omega\phi_2^*(\omega)\hat{a}_i^\dagger(\omega)e^{i\omega(T+\tau)}|0\rangle, i = 1,2$ only indicates whether the photon is in output mode a_1 or a_2. $\Delta\omega = |\overline{\omega}_b - \overline{\omega}_a| = \omega_2 - \omega_1$ is the central frequency difference between the two photons. We define a new state as $|\Psi_{\text{ent}}^{'}\rangle = e^{i\xi}|\Psi_{\text{ent}}\rangle$. Because the factor $e^{i\xi}$ disappears in Eq. (A7) and has no influence on the detected result, for convenience, we still write $|\Psi_{\text{ent}}^{'}\rangle$ as $|\Psi_{\text{ent}}\rangle$.

[1] E. Knill, R. Laflamme, and G. J. Milburn, Nature (London) **409**, 46 (2001).
[2] M. Zukowski, A. Zeilinger, M. A. Horne, and A. K. Ekert, Phys. Rev. Lett. **71**, 4287 (1993).
[3] J.-W. Pan, D. Bouwmeester, H. Weinfurter, and A. Zeilinger, Phys. Rev. Lett. **80**, 3891 (1998).
[4] H. J. Kimble, Nature (London) **453**, 1023 (2008).
[5] C. K. Hong, Z.-Y. Ou, and L. Mandel, Phys. Rev. Lett. **59**, 2044 (1987).
[6] H. de Riedmatten, I. Marcikic, W. Tittel, H. Zbinden, and N. Gisin, Phys. Rev. A **67**, 022301 (2003).
[7] J.-W. Pan, Z.-B. Chen, C.-Y. Lu, H. Weinfurter, A. Zeilinger, and M. Żukowski, Rev. Mod. Phys **84**, 777 (2012).
[8] O. Cohen, J. S. Lundeen, B. J. Smith, G. Puentes, P. J. Mosley, and I. A. Walmsley, Phys. Rev. Lett. **102**, 123603 (2009).
[9] V. Balić, D. A. Braje, P. Kolchin, G. Y. Yin, and S. E. Harris, Phys. Rev. Lett. **94**, 183601 (2005).
[10] S. Du, J. Wen, and M. H. Rubin, J. Opt. Soc. Am. B **25**, C98 (2008).
[11] B. Srivathsan, G. K. Gulati, B. Chng, G. Maslennikov, D. Matsukevich, and C. Kurtsiefer, Phys. Rev. Lett. **111**, 123602 (2013).
[12] J. F. Chen and S. Du, Front. Phys. **7**, 494 (2012).
[13] R. Kaltenbaek, B. Blauensteiner, M. Żukowski, M. Aspelmeyer, and A. Zeilinger, Phys. Rev. Lett. **96**, 240502 (2006).
[14] P. Maunz, D. Moehring, S. Olmschenk, K. Younge, D. Matsukevich, and C. Monroe, Nat. Phys. **3**, 538 (2007).
[15] P. Qian, Z. Gu, R. Cao, R. Wen, Z. Y. Ou, J. F. Chen, and W. Zhang, Phys. Rev. Lett. **117**, 013602 (2016).
[16] C. Söller, O. Cohen, B. J. Smith, I. A. Walmsley, and C. Silberhorn, Phys. Rev. A **83**, 031806 (2011).
[17] J. Beugnon, M. P. Jones, J. Dingjan, B. Darquié, G. Messin, A. Browaeys, and P. Grangier, Nature (London) **440**, 779 (2006).
[18] R. B. Patel, A. J. Bennett, I. Farrer, C. A. Nicoll, D. A. Ritchie, and A. J. Shields, Nat. Photon. **4**, 632 (2010).
[19] H. Bernien, L. Childress, L. Robledo, M. Markham, D. Twitchen, and R. Hanson, Phys. Rev. Lett. **108**, 043604 (2012).
[20] V. Leong, S. Kosen, B. Srivathsan, G. K. Gulati, A. Cerè, and C. Kurtsiefer, Phys. Rev. A **91**, 063829 (2015).
[21] J. Dodd, W. Sandle, and D. Zissermann, Proc. Phys. Soc. **92**, 497 (1967).
[22] A. Aspect, J. Dalibard, P. Grangier, and G. Roger, Opt. Commun. **49**, 429 (1984).
[23] G. K. Gulati, B. Srivathsan, B. Chng, A. Cerè, and C. Kurtsiefer, New J. Phys. **17**, 093034 (2015).
[24] M. Schug, C. Kurz, P. Eich, J. Huwer, P. Müller, and J. Eschner, Phys. Rev. A **90**, 023829 (2014).
[25] Z. Y. Ou and L. Mandel, Phys. Rev. Lett. **61**, 54 (1988).
[26] S. Ramelow, L. Ratschbacher, A. Fedrizzi, N. K. Langford, and A. Zeilinger, Phys. Rev. Lett. **103**, 253601 (2009).
[27] A. Fedrizzi, T. Herbst, M. Aspelmeyer, M. Barbieri, T. Jennewein, and A. Zeilinger, New J. Phys. **11**, 103052 (2009).
[28] T. Legero, T. Wilk, A. Kuhn, and G. Rempe, Appl. Phys. B **77**, 797 (2003).
[29] Z. Han, P. Qian, L. Zhou, J. F. Chen, and W. Zhang, Sci. Rep. **5**, 9126 (2015).
[30] A. Cerè, V. Leong, S. Kosen, B. Srivathsan, G. K. Gulati, and C. Kurtsiefer, in *Proceedings of SPIE, Quantum Communications and Quantum Imaging XIII* (SPIE Optical Engineering + Applications, San Diego, California, 2015), Vol. 9615, p. 96150Q.
[31] R. Lettow, Y. L. A. Rezus, A. Renn, G. Zumofen, E. Ikonen, S. Götzinger, and V. Sandoghdar, Phys. Rev. Lett. **104**, 123605 (2010).
[32] Y.-W. Lin, H.-C. Chou, P. P. Dwivedi, Y.-C. Chen, and I. A. Yu, Opt. Express **16**, 3753 (2008).
[33] S. Zhang, J. Chen, C. Liu, S. Zhou, M. M. Loy, G. K. Wong, and S. Du, Rev. Sci. Instrum. **83**, 073102 (2012).
[34] L. Zhao, X. Guo, C. Liu, Y. Sun, M. M. T. Loy, and S. Du, Optica **1**, 84 (2014).

[35] S. Du, Phys. Rev. A **92**, 043836 (2015).
[36] M. Eisaman, A. André, F. Massou, M. Fleischhauer, A. Zibrov, and M. Lukin, Nature (London) **438**, 837 (2005).
[37] Z. Jun, G. Zhen-Jie, Q. Peng, H. Zhi-Guang, and C. Jie-Fei, Chin. Phys. Lett. **32**, 064211 (2015).
[38] Y. F. Hsiao, H. S. Chen, P. J. Tsai, and Y. C. Chen, Phys. Rev. A **90**, 055401 (2014).
[39] P. G. Kwiat, K. Mattle, H. Weinfurter, A. Zeilinger, A. V. Sergienko, and Y. Shih, Phys. Rev. Lett. **75**, 4337 (1995).
[40] X. Guo, Y. Mei, and S. Du, Optica **4**, 388 (2017).
[41] T. Legero, T. Wilk, M. Hennrich, G. Rempe, and A. Kuhn, Phys. Rev. Lett. **93**, 070503 (2004).
[42] T.-M. Zhao, H. Zhang, J. Yang, Z.-R. Sang, X. Jiang, X.-H. Bao, and J.-W. Pan, Phys. Rev. Lett. **112**, 103602 (2014).
[43] S. Clemmen, A. Farsi, S. Ramelow, and A. L. Gaeta, Phys. Rev. Lett. **117**, 223601 (2016).
[44] M. Halder, A. Beveratos, N. Gisin, V. Scarani, C. Simon, and H. Zbinden, Nat. Phys. **3**, 692 (2007).